Journal of Mechanical Engineering Research Vol. 4(3), pp. 100-111, March 2012
Available online at http://www.academicjournals.org/JMER
DOI: 10.5897/JMER11.074
ISSN 2141-2383 ©2012 Academic Journals

Full Length Research Paper

Evaluation of the turbulence models for the simulation of the flow over a National Advisory Committee for Aeronautics (NACA) 0012 airfoil

Douvi C. Eleni*, Tsavalos I. Athanasios and Margaris P. Dionissios

Department of Mechanical Engineering and Aeronautics, Fluid Mechanics Laboratory (FML), University of Patras, 26500 Patras, Greece.

Accepted 14 February, 2012

The analysis of the two dimensional subsonic flow over a National Advisory Committee for Aeronautics (NACA) 0012 airfoil at various angles of attack and operating at a Reynolds number of 3×10^6 is presented. The flow was obtained by solving the steady-state governing equations of continuity and momentum conservation combined with one of three turbulence models [Spalart-Allmaras, Realizable $k-\varepsilon$ and $k-\omega$ shear stress transport (SST)] aiming to the validation of these models through the comparison of the predictions and the free field experimental measurements for the selected airfoil. The aim of the work was to show the behavior of the airfoil at these conditions and to establish a verified solution method. The computational domain was composed of 80000 cells emerged in a structured way, taking care of the refinement of the grid near the airfoil in order to enclose the boundary layer approach. Calculations were done for constant air velocity altering only the angle of attack for every turbulence model tested. This work highlighted two areas in computational fluid dynamics (CFD) that require further investigation: transition point prediction and turbulence modeling. The laminar to turbulent transition point was modeled in order to get accurate results for the drag coefficient at various Reynolds numbers. In addition, calculations showed that the turbulence models used in commercial CFD codes does not give yet accurate results at high angles of attack.

Key words: Computational fluid dynamics (CFD), airfoil, aerodynamic coefficients, lift, drag, turbulence models, transition point.

INTRODUCTION

The rapid evolution of computational fluid dynamics (CFD) has been driven by the need for faster and more accurate methods for the calculations of flow fields around configurations of technical interest. In the past decade, CFD was the method of choice in the design of many aerospace, automotive and industrial components and processes in which fluid or gas flows play a major role. In the fluid dynamics, there are many commercial CFD packages available for modeling flow in or around objects. The computer simulations show features and details that are difficult, expensive or impossible to measure or visualize experimentally.

When simulating the flow over airfoils, transition from laminar to turbulent flow plays an important role in determining the flow features and in quantifying the airfoil performance such as lift and drag. Hence, the proper modeling of transition, including both the onset and extent of transition will definitely lead to a more accurate drag prediction. Bacha et al. (2006) presented a transition model that combined existing methods for predicting the onset and extent of transition, which were compatible with the Spalart-Allmaras turbulence model, where the

*Corresponding author. E-mail: douvi@mech.upatras.gr. Tel: +30 2610997193. Fax: +30 2610997202.

Abbreviations: CFD, Computational fluid dynamics; C_L, coefficient of lift; C_D, coefficient of drag; **Re,** Reynolds number; **a,** angle of attack; **SST,** shear stress transport.

flow was simulated using Fluent. The onset of transition is based on Michel's method for incompressible two-dimensional flow while the extent of transition is quantified by developing a model for the intermittency function. Badran (2008) tested two-equation turbulence models [Realizable and RNG $k-\varepsilon$ models and the Reynolds stress model (RSM)] for the ability to predict boundary layer separation on National Advisory Committee for Aeronautics (NACA) 4412 airfoil at the position of maximum lift. Ma (2010) carried out 2D numerical simulation for S825 and S827 wind turbine airfoils with three different turbulence models (Spalart-Allmaras, standard $k-\varepsilon$ and standard $k-\omega$).

The first step in modeling a problem involves the creation of the geometry and the meshes with a preprocessor. The majority of time spent on a CFD project in the industry is usually devoted to successfully generating a mesh for the domain geometry that allows a compromise between desired accuracy and solution cost. After the creation of the grid, a solver is able to solve the governing equations of the problem. The basic procedural steps for the solution of the problem are the following. First, the modeling goals have to be defined and the model geometry and grid are created. Then, the solver and the physical models are stepped up in order to compute and monitor the solution. Afterwards, the results are examined and saved and if it is necessary we consider revisions to the numerical or physical model parameters.

In this project, curves for the lift and drag characteristics of the NACA 0012 airfoil were developed. This airfoil was chosen because it has been used in many constructions. Typical examples of such use of the airfoil are the B-17 Flying Fortress and Cessna 152, the helicopter Sikorsky S-61 SH-3 Sea King as well as horizontal and vertical axis wind turbines.

Dependence of the drag C_D and lift coefficient C_L on the angle of attack was determined using three different turbulence models. Turbulent flows are significantly affected by the presence of walls, where the viscosity – affected regions have large gradients in the solution variables and accurate presentation of the near wall region determines successful prediction of wall bounded turbulent flows. The aim of this project was to find the most appropriate turbulence model for this simulation. In fluid dynamics, turbulence or turbulent flow is a fluid regime characterized by chaotic, stochastic property changes. This includes low momentum diffusion, high momentum convection and rapid variation of pressure and velocity in space and time.

In this analysis, the Spalart-Allmaras model, the realizable $k-\varepsilon$ model and the shear stress transport (SST) $k-\omega$ model were combined with the governing equations for the numerical solution of the flow field over the NACA 0012 airfoil and existing experimental data from reliable sources (Abbott et al., 1959) are performed to validate the computational results. In order to include the transition effects in the aerodynamic coefficients calculation and get accurate results for the drag coefficient, a new method was used. The first step of the method was used for determining the transition point from laminar to turbulent flow on the airfoil and in a second step the computational mesh was split in two regions, a laminar and a turbulent region.

MATHEMATICAL FORMULATION AND TURBULENCE MODELS

For all flows, the solver solves conservation equations for mass and momentum. Additional transport equations are also solved when the flow is turbulent. The equation for conservation of mass or continuity equation, can be written as follows:

$$\frac{\partial \rho}{\partial t} + \nabla \cdot \left(\rho \vec{u}\right) = S_m \quad (1)$$

Equation 1 is the general form of the mass conservation equation and is valid for incompressible as well as compressible flows. The source S_m is the mass added to the continuous phase from the dispersed second phase (for example, due to vaporization of liquid droplets) and any user-defined sources. Conservation of momentum in an inertial reference frame is described by Equation 2

$$\frac{\partial}{\partial t}\left(\rho \vec{u}\right) + \nabla \cdot \left(\rho \vec{u}\vec{u}\right) = -\nabla p + \nabla \cdot \left(\bar{\bar{\tau}}\right) + \rho \vec{g} + \vec{F} \quad (2)$$

where p is the static pressure, $\bar{\bar{\tau}}$ is the stress tensor (described below) and $\rho \vec{g}$ and $\vec{F}$ are the gravitational body force and external body forces (for example, that arise from interaction with the dispersed phase), respectively. $\vec{F}$ also contains other model-dependent source terms such as porous-media and user-defined sources. The stress tensor $\bar{\bar{\tau}}$ is given by:

$$\bar{\bar{\tau}} = \mu\left[\left(\nabla \vec{u} + \nabla \vec{u}^T\right) - \frac{2}{3}\right]\nabla \cdot \vec{u} I \quad (3)$$

where μ is the molecular viscosity, I is the unit tensor, and the second term on the right hand side is the effect of volume dilation.

For the 2-D, steady and incompressible flow the continuity equation is:

$$\frac{\partial u}{\partial x} + \frac{\partial v}{\partial y} = 0 \quad (4)$$

Momentum equations for viscous flow in x and y

directions are, respectively:

$$\rho\frac{Du}{Dt}=-\frac{\partial p}{\partial x}+\frac{\partial \tau_{xx}}{\partial x}+\frac{\partial \tau_{yx}}{\partial y}+\rho f_x \quad (5)$$

$$\rho\frac{Dv}{Dt}=-\frac{\partial p}{\partial y}+\frac{\partial \tau_{xy}}{\partial x}+\frac{\partial \tau_{yy}}{\partial y}+\rho f_y \quad (6)$$

where due to characteristics of the 2-D flow in continuity equation the term $\partial w/\partial z$ and in momentum equation, $\partial \tau_{zx}/\partial z$ and $\partial \tau_{zy}/\partial z$ drop out. The continuity and momentum equations are combined with one of the following turbulence model which are briefly presented as follows:

The Spalart-Allmaras turbulence model

The Spalart and Allmaras (1992) model is a relatively simple one-equation model that solves a modelled transport equation for the kinematic eddy (turbulent) viscosity. It was designed specifically for aerospace applications involving wall-bounded flows and has been shown to give good results for boundary layers subjected to adverse pressure gradients. It is also gaining popularity for turbo machinery applications. In its original form, it is effectively a low-Reynolds number model, requiring the viscous-affected region of the boundary layer to be properly resolved. The near-wall gradients of the transported variable in the model are much smaller than the gradients of the transported variables in the $k-\varepsilon$ or $k-\omega$ models. In the turbulence model of Spalart-Allmaras the transport equation can be written in

$$\frac{\mathrm{D}\tilde{\nu}}{\mathrm{D}t}=c_{b1}(1-f_{t2})\tilde{S}\tilde{\nu}+\frac{1}{\sigma}\left[\nabla\cdot\left((\nu+\tilde{\nu})\right)\nabla\tilde{\nu}+c_{b2}(\nabla\tilde{\nu})^2\right]-\left(c_{w1}f_w-\frac{c_{b1}}{\kappa^2}f_{t2}\right)\left(\frac{\tilde{\nu}}{d}\right)^2+f_{t1}\Delta U^2 \quad (7)$$

the form of the operating parameter $\tilde{\nu}$, as belows:where ν is the molecular viscosity calculated by the Sutherland's (1893) law. The four terms on the right hand side correspond to production, diffusion, dissipation and transition, respectively. The individual components of the production term are defined as:

$$\tilde{S}\equiv S+\frac{\tilde{\nu}}{\kappa^2 d^2}\left[1-(\tilde{\nu}/\nu)\left[1+\frac{(\tilde{\nu}/\nu)^4}{\left[(\tilde{\nu}/\nu)^3+C_{v1}^3\right]}\right]^{-1}\right] \quad (8)$$

$$f_w=\frac{\tilde{\nu}}{\tilde{S}k^2d^2}\left[1+C_{w2}\left(\left(\frac{\tilde{\nu}}{\tilde{S}k^2d^2}\right)^5-1\right)\right]\left(1+C_{w3}^6\right)^{1/6}\left\{\left[1+C_{w2}\left(\left(\frac{\tilde{\nu}}{\tilde{S}k^2d^2}\right)^5-1\right)\right]^6+C_{w3}^6\right\}^{-1/6} \quad (9)$$

$$f_{t1}=C_{t1}g_t\exp\left[-C_{t2}\frac{\omega_t^2}{\Delta U^2}\left(d^2+g_t^2d_t^2\right)\right],\quad f_{t2}=C_{t3}\exp\left[-C_{t4}(\tilde{\nu}/\nu)^2\right] \quad (10)$$

where S is the magnitude of the vorticity, d is the distance to the closest wall, d_t is the distance from the point in the flow field to the trip on the wall, ω_t is the wall vorticity at the trip, ΔU is the difference between velocity at the field point and that at the trip, $g_t=\min(0.1,\Delta U/\omega_t\Delta x_t)$ where Δx_t is the grid spacing along the wall at the trip. The empirical constants of the Spalart-Allmaras model are: $C_{b1}=0.1355$, $\sigma=2/3$, $C_{b2}=0.622$, $\kappa=0.4187$, $C_{w1}=3.239$, $C_{w2}=0.3$, $C_{w3}=2.0$, $C_{v1}=7.1$, $C_{t1}=1$, $C_{t2}=2$, $C_{t3}=1.2$ and $C_{t4}=0.5$.

The Realizable $k-\varepsilon$ turbulence model

The simplest "complete models" of turbulence are two-equation models in which the solution of two separate transport equations allows the turbulent velocity and length scales to be independently determined. The standard $k-\varepsilon$ model falls within this class of turbulence model and has become the workhorse of practical engineering flow calculations in the time since it was proposed by Launder and Spalding (1974). Robustness, economy and reasonable accuracy for a wide range of turbulent flows explain its popularity in industrial flow and heat transfer simulations.

It is a semi-empirical model and the derivation of the

model equations relies on phenomenological considerations and empiricism. As the strengths and weaknesses of the standard $k-\varepsilon$ model have become known, improvements have been made to the model to improve its performance. Two of these variants are available: the RNG $k-\varepsilon$ model and the Realizable $k-\varepsilon$ model (Shih et al., 1995).

The modelled transport equations for k and ε in the realizable $k-\varepsilon$ model are:

$$\frac{\partial}{\partial t}(\rho k)+\frac{\partial}{\partial x_j}(\rho k u_j)=\frac{\partial}{\partial x_j}\left[\left(\mu+\frac{\mu_t}{\sigma_k}\right)\frac{\partial k}{\partial x_j}\right]+G_k+G_b-\rho\varepsilon-Y_M+S_k \quad (11)$$

And

$$\frac{\partial}{\partial t}(\rho\varepsilon)+\frac{\partial}{\partial x_j}(\rho\varepsilon u_j)=\frac{\partial}{\partial x_j}\left[\left(\mu+\frac{\mu_t}{\sigma_\varepsilon}\right)\frac{\partial \varepsilon}{\partial x_j}\right]+\rho C_1 S\varepsilon-\rho C_2\frac{\varepsilon^2}{k+\sqrt{\nu\varepsilon}}+C_{1\varepsilon}\frac{\varepsilon}{k}C_{3\varepsilon}G_b+S_\varepsilon \quad (12)$$

where

$$C_1=\max\left[0.43,\frac{n}{n+5}\right], n=S\frac{k}{\varepsilon}, S=\sqrt{2S_{ij}S_{ij}} \quad (13)$$

In these equations, G_k represents the generation of turbulence kinetic energy due to the mean velocity gradients. G_b is the generation of turbulence kinetic energy due to buoyancy. Y_M represents the contribution of the fluctuating dilatation in compressible turbulence to the overall dissipation rate ($Y_M=2\rho\varepsilon M_t^2$, where M_t is the turbulent Mach number). C_2 and $C_{1\varepsilon}$ are constants. σ_k and σ_ε are the turbulent Prandtl numbers for k and ε, respectively. S_k and S_ε are user-defined source terms. The constants of the Realizable $k-\varepsilon$ model are: $C_{1\varepsilon}=1.44$, $C_2=1.9$, $\sigma_k=1.0$ and $\sigma_\varepsilon=1.2$.

The $k-\omega$ SST turbulence model

The standard $k-\omega$ model is based on the Wilcox (1988) $k-\omega$ model, which incorporates modifications for low-Reynolds number effects, compressibility and shear flow spreading. The Wilcox model predicts free shear flow spreading rates that are in close agreement with measurements for far wakes, mixing layers and plane, round, and radial jets, and is thus applicable to wall-bounded flows and free shear flows. A variation of the standard $k-\omega$ model called the $k-\omega$ SST model is also available. The $k-\omega$ SST model was developed by Menter (1994) to effectively blend the robust and accurate formulation of the $k-\omega$ model in the near-wall region with the free-stream independence of the $k-\varepsilon$ model in the far field. To achieve this, the $k-\varepsilon$ model is converted into a $k-\omega$ formulation. The $k-\omega$ SST model is similar to the standard $k-\omega$ model, but includes some refinements. These features make the $k-\omega$ SST model more accurate and reliable for a wider class of flows (for example, adverse pressure gradient flows, airfoils, transonic shock waves) than the standard $k-\omega$ model. The $k-\omega$ SST turbulence model is a combined version of the $k-\varepsilon$ and the $k-\omega$ turbulence models and is governed by:

$$\frac{\mathrm{D}\rho k}{\mathrm{D}t}=\tau_{ij}\frac{\partial u_i}{\partial x_j}+\beta^*\rho\omega k+\frac{\partial}{\partial x_j}\left[(\mu+\sigma_k\mu_t)\frac{\partial k}{\partial x_j}\right] \quad (14)$$

$$\frac{\mathrm{D}\rho\omega}{\mathrm{D}t}=\frac{\gamma}{\nu_t}\tau_{ij}\frac{\partial u_i}{\partial x_j}-\beta\rho\omega^2+\frac{\partial}{\partial x_j}\left[(\mu+\sigma_\omega\mu_t)\frac{\partial\omega}{\partial x_j}\right]+2\rho(1-F_1)\sigma_\omega\frac{1}{\omega}\frac{\partial k}{\partial x_j}\frac{\partial\omega}{\partial x_j} \quad (15)$$

Where $\beta^*=\varepsilon/k\omega$ and the turbulence stress tensor is

$$\tau_{ij}=-\rho\overline{u_i'u_j'}=\mu_t\left(\frac{\partial u_i}{\partial x_j}+\frac{\partial u_j}{\partial x_i}-\frac{2}{3}\frac{\partial u_k}{\partial x_k}\delta_{ij}\right)-\frac{2}{3}\rho k\delta_{ij} \quad (16)$$

The turbulence viscosity can be estimated by $\nu_t=a_1k/\max(a_1\omega,\Omega F_2)$, where Ω is the absolute value of the vorticity, $a_1=0.31$ and the function F_2 is given by

$$F_2=\tanh\left\{\left[\max\left(\frac{2\sqrt{k}}{0.09\omega y},\frac{500\nu}{y^2\omega}\right)\right]\right\}^2 \quad (17)$$

Where y is the distance to the nearest surface.

The coefficients β,γ,σ_k and σ_ω are defined as

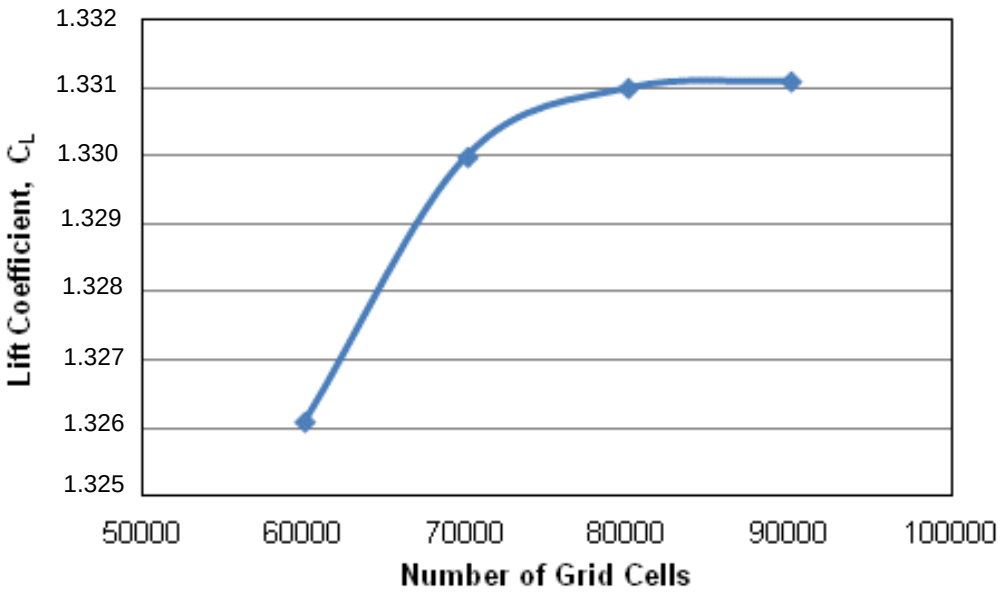

Figure 1. Curve of lift coefficient at stall angle of attack against number of grid cells.

functions of the coefficients of the $k-\omega$ and $k-\varepsilon$ turbulence models and they are listed as follows:

$$\beta = F_1\beta_1 + (1-F_1)\beta_2,\ \gamma = F_1\gamma_1 + (1-F_1)\gamma_2,$$
$$\sigma_k = F_1\sigma_{k1} + (1-F_1)\sigma_{k2},\ \sigma_\omega = F_1\sigma_{\omega 1} + (1-F_1)\sigma_{\omega 2} \quad (18)$$

where the function F_1 is

$$F_1 = \tanh\left\{\left[\min\left[\max\left(\frac{\sqrt{k}}{0.09\omega y}, \frac{500v}{y^2\omega}\right), \frac{4\rho\sigma_{\omega 2}k}{CD_{k\omega}y^2}\right]\right]^4\right\} \quad (19)$$

and the coefficient $CD_{k\omega}$ is

$$CD_{k\omega} = \max\left(2\rho\sigma_{\omega 2}\frac{1}{\omega}\frac{\partial k}{\partial x_j}\frac{\partial \omega}{\partial x_j}, 10^{-20}\right) \quad (20)$$

The empirical constants of the $k-\omega$ SST model are: $\beta^* = 0.09$, $\beta_1 = 0.075$, $\beta_2 = 0.0828$, $\gamma_1 = 0.5532$, $\gamma_2 = 0.4404$, $\sigma_{k1} = 0.85$, $\sigma_{k2} = 1.0$, $\sigma_{\omega 1} = 0.5$ and $\sigma_{\omega 2} = 0.856$.

Computational method

In this paper, the NACA 0012, the well documented airfoil from the 4-digit series of NACA airfoils, was utilized. The NACA 0012 airfoil is symmetrical; the 00 indicates that it has no camber. The 12 indicates that the airfoil has a 12% thickness to chord length ratio; it is 12% as thick as it is long. Reynolds number for the simulations was $Re=3x10^6$, same with the reliable experimental data from Abbott and Von Doenhoff (1959), in order to validate the present simulation. The free stream temperature is 300 K, which is the same as the environmental temperature. The density of the air at the given temperature is $\rho=1.225kg/m^3$ and the viscosity is $\mu=1.7894\times10^{-5}kg/ms$. For this Reynolds number, the flow can be described as incompressible. This is an assumption close to reality and it is not necessary to resolve the energy equation. A segregated, implicit solver was utilized (ANSYS Fluent 6.3.26., 2006) Calculations were done for angles of attack ranging from -12 to 20°. The airfoil profile, boundary conditions and meshes were all created in the pre-processor Gambit 2.4.6. The pre-processor is a program that can be employed to produce models in two and three dimensions, using structured or unstructured meshes, which can consist of a variety of elements, such as quadrilateral, triangular or tetrahedral elements. The resolution of the mesh was greater in regions where greater computational accuracy was needed, such as the region close to the airfoil.

The first step in performing a CFD simulation should be to investigate the effect of the mesh size on the solution results. Generally, a numerical solution becomes more accurate as more nodes are used, but using additional nodes also increases the required computer memory and computational time. The appropriate number of nodes can be determined by increasing the number of nodes until the mesh is sufficiently fine so that further refinement does not change the results. Figure 1 shows the effect of number of grid cells in coefficient of lift at stall angle of attack (16°).

This study revealed that a C-type grid topology with 80000 quadrilateral cells would be sufficient to establish a grid independent solution (Figure 2). The domain height was set to approximately 20 chord lengths and the height of the first cell adjacent to the surface was set to 10^{-5}, corresponding to a maximum y^+ of approximately 0.2. A y^+ of this size should be sufficient to properly resolve the inner parts of the boundary layer

In order to include the transition effects in the aerodynamic coefficients calculation and get accurate results for the drag coefficient, a new method was used. The transition point from laminar to turbulent flow on the airfoil was determined and the computational mesh was split in two regions, a laminar and a

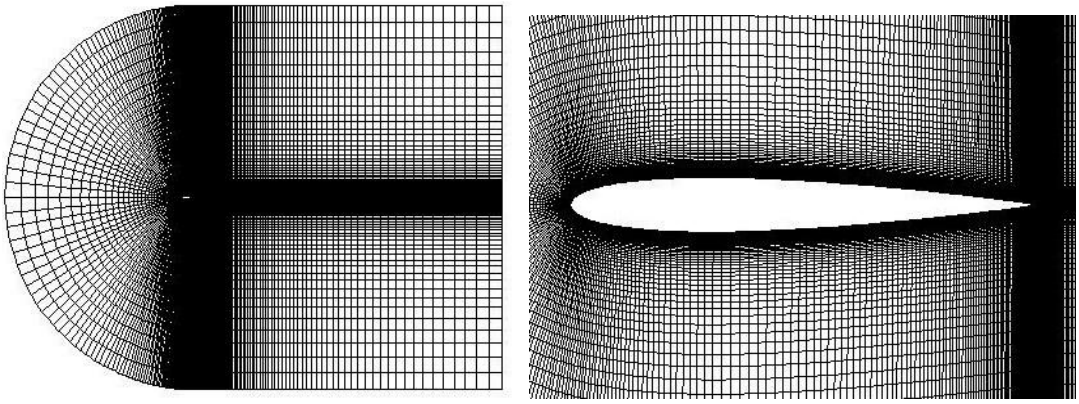

Figure 2. Mesh around NACA 0012 airfoil (left) and detail closed to the airfoil (right).

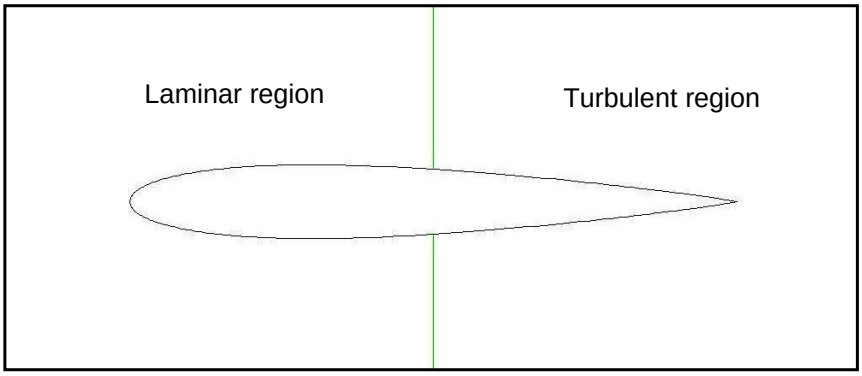

Figure 3. Flow regions around the airfoil.

turbulent region. To calculate the transition point the following procedure was used. A random value for the transition point (x_{tr}) was chosen and the computational domain was split at that point with a perpendicular line. The problem was simulated in Fluent after defining the left region as laminar and the right as turbulent zone, as shown in Figure 3.

If the C_D simulation result was larger than the experimental data it meant that the simulated turbulent zone was larger than the real and a new value for the transition point had to be chosen, righter than the initial one. Respectively, if the C_D simulation result was lower than the experimental data it meant that the simulated turbulent zone was smaller than the real and the transition point was more left. This procedure was repeated until two C_D simulated results came of, which should satisfy the inequality $C_{D,sim1} < C_{D,\exp} < C_{D,sim2}$ and $x_{tr1}<x_{tr}<x_{tr2}$. The linear interpolation of the mentioned values results the correct x_{tr}. The mesh was separated with the x_{tr} that was calculated in two regions as mentioned earlier and the simulated results were closer to the experimental data.

RESULTS AND DISCUSSION

Simulations for various angles of attack were done in order to be able to compare the results from the different turbulence models and then validate them with existing experimental data from reliable sources. To do so, the model was solved with a range of different angles of attack from -12 to 20°.

On an airfoil, the resultants of the forces are usually resolved into two forces and one moment. The component of the net force acting normal to the incoming flow stream is known as the lift force and the component of the net force acting parallel to the incoming flow stream is known as the drag force. The curves of the lift and the drag coefficient are shown for various angles of attack, computed with three turbulence models and compared with experimental data.

Figure 4 shows that at low angles of attack, the dimensionless lift coefficient increased linearly with angle of attack. Flow was attached to the airfoil throughout this regime. At an angle of attack of roughly 15 to 16°, the flow on the upper surface of the airfoil began to separate and a condition known as stall began to develop. All three models had a good agreement with the experimental data at angles of attack from -10 to 10° and the same behavior at all angles of attack until stall. It was obvious that the Spalart-Allmaras turbulence model had the same behaviour with the experimental data as well as after

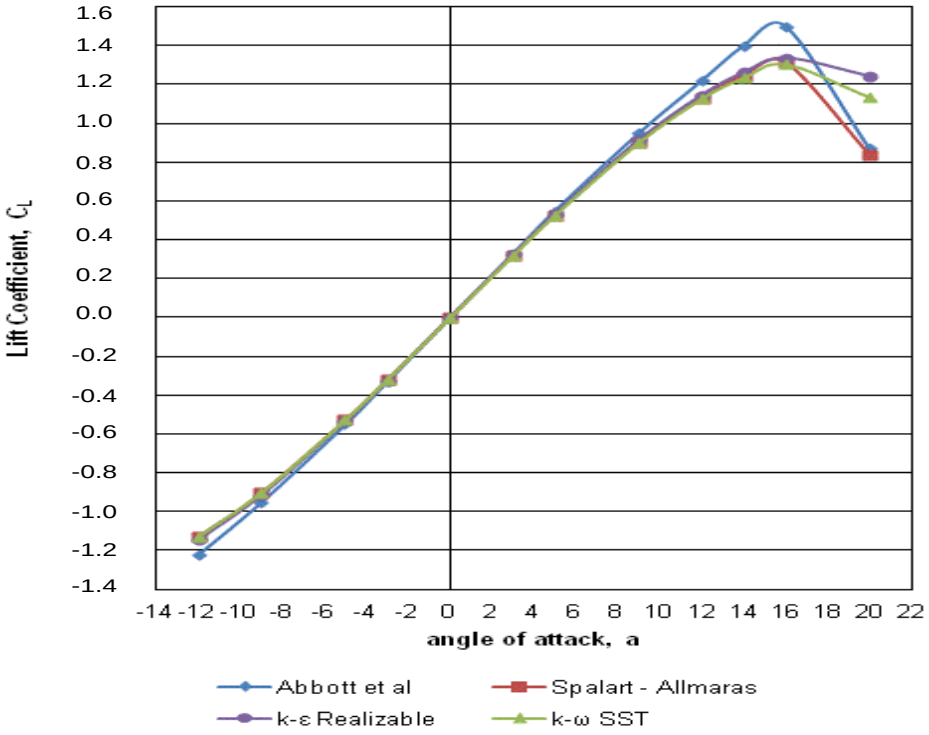

Figure 4. Comparison between experimental data from Abbott et al and three different turbulent models simulation results of the lift coefficient curve for NACA 0012 airfoil.

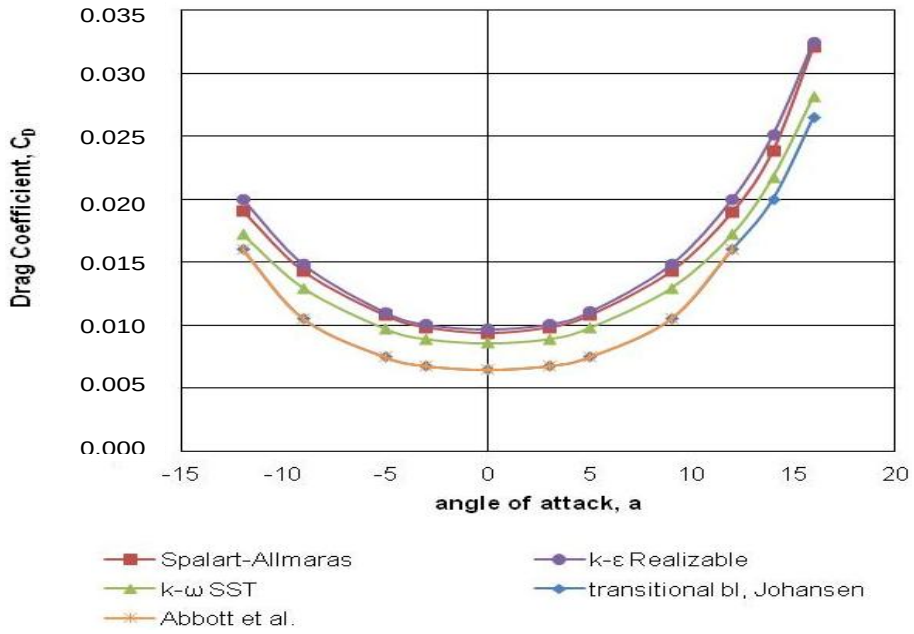

Figure 5. Comparison between experimental data from Abbott and Von Doenhoff (1959) and Johansen (1997) for transitional boundary layer and three different turbulent models simulation results of the drag coefficient curve for NACA 0012 airfoil.

stall angle.

Near stall, disagreement between the data was shown. The lift coefficient peaked and the drag coefficient increased as stall increased. The predicted drag coefficients were higher than the experimental data (Figure 5). This over prediction of drag was expected

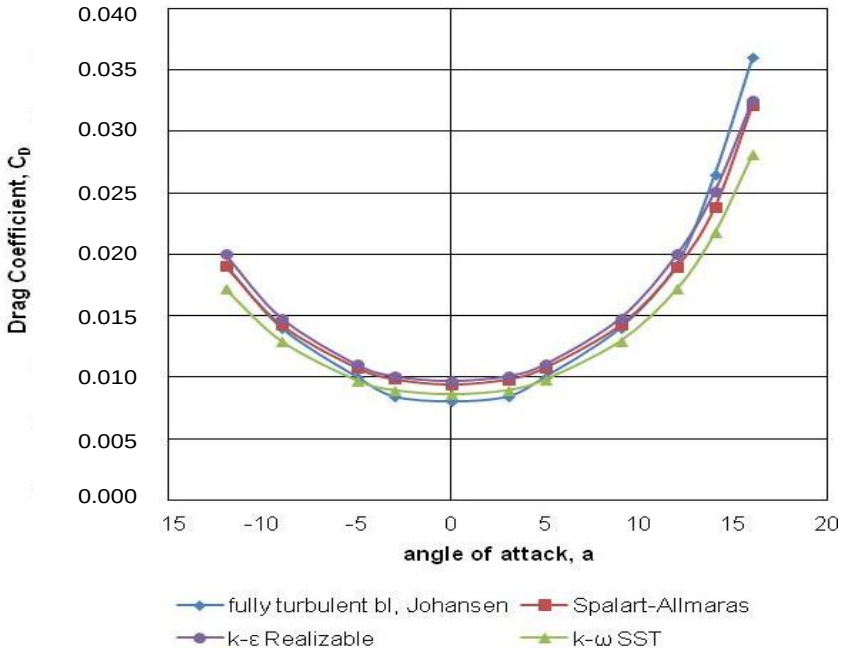

Figure 6. Comparison between experimental data for fully turbulent boundary layer from Johansen and three different turbulent models simulation results of the drag coefficient curve for NACA 0012 airfoil.

since the actual airfoil has laminar flow over the forward half. The turbulence models cannot calculate the transition point from laminar to turbulent and consider that the boundary layer is turbulent throughout its length. From theory, the turbulent boundary layer carries more energy and C_D is much greater than at the viscous boundary layer, which carries less energy. The computational results must be compared with experimental data of a fully turbulent boundary layer. This was done only for C_D as C_L is less sensitive to the transition point.

Johansen (1997) contained experimental data of C_D for the NACA 0012 airfoil and Re=3×10^6, where the boundary layer formed around the airfoil is fully turbulent. Figure 6 shows the curves of C_D for various angles of attack, compared with experimental data for fully turbulent boundary layer. The values of C_D from the three turbulence models were very close to experimental data for the fully turbulent boundary layer. The most accurate model was the $k-\omega$ SST model, second came the Spalart-Allmaras and latest in precision was the Realizable $k-\varepsilon$.

In order to get more accurate results, the computational domain could be split into two different domains to run mixed laminar and turbulent flow. The disadvantages of this approach were that the accuracy of simulations depends on the ability to accurately guess the transition location, and a new grid must be generated if thetransition point had to change (Silisteanu-Botez, 2010). If the transition point is known, the grid can easily be split in two with a vertical line that passes through this point and then laminar and turbulent zones are defined. The results of this method at angle of attack a=0 and operating at Re = 1×10^6, 2×10^6, 3×10^6, 4×10^6 and 5×10^6 are shown in Figure 7. Initially, C_D was calculated for a fully turbulent boundary layer and compared with experimental data from NASA (McCroskey, 1987). Then, simulations were made with the split grid for the five Reynolds numbers. The computational results for the fully turbulent boundary layer agreed very well with the corresponding experimental data. The discrepancy between the drag coefficient numerical and experimental values from McCroskey for fully turbulent boundary layer was up to 5.6%. On the other hand, the comparison between the simulation results with the split grid and the experimental data from McCroskey for transitional boundary layer showed an excellent agreement, with maximum error of about 3.6%. It is obvious that a better drag prediction was observed for the present methodology with the split grid.

It was also observed that as the Reynolds number increased the drag coefficient decreased. When the boundary layer was fully turbulent the reduction of C_D was more intense and when there was a transition from laminar to turbulent, C_D was reduced to a much lower rate. It is worth noting that this process of calculating the transition point is quite simple when the angle of attack is

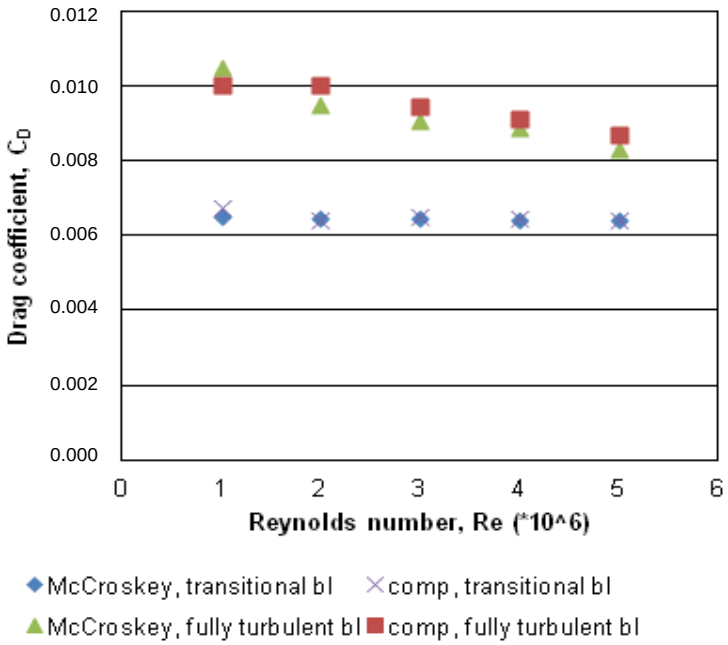

Figure 7. Comparison between experimental data for fully turbulent and transitional boundary layer from McCroskey and simulation results with the split grid of the drag coefficient curve for NACA 0012 airfoil at zero angle of attack and at various Reynolds numbers.

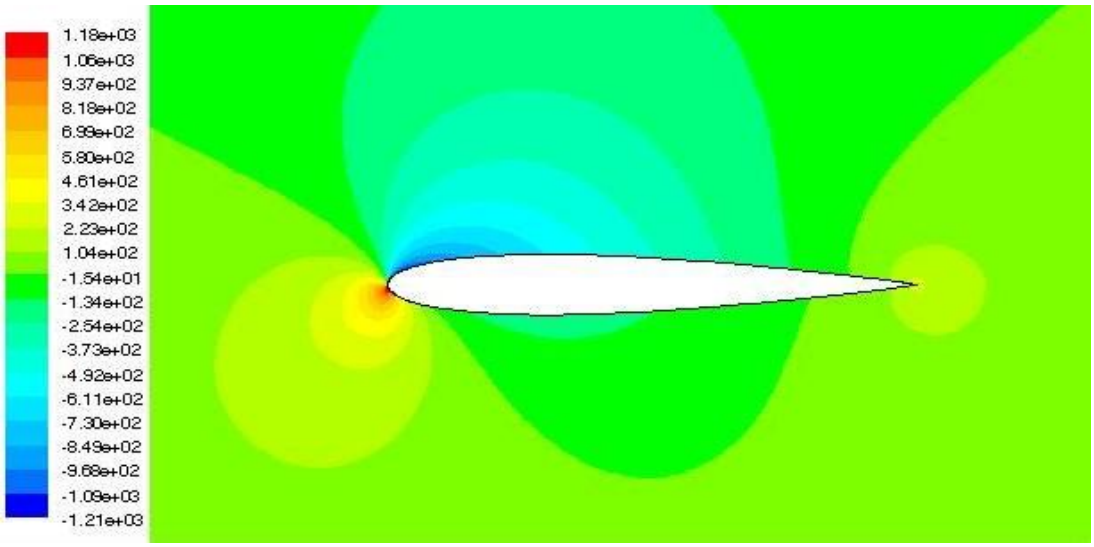

Figure 8. Contours of static pressure at 3° angle of attack with the Spalart – Allmaras turbulence model.

zero because the flow is symmetric and the transition point is the same above and below the airfoil. At nonzero angles of attack the process is more complicated because transition points are different for the upper and lower surface of the airfoil.

Figures 8 and 9 shows the simulation outcomes of static pressure at angles of attack 3 and 9° with the Spalart-Allmaras turbulence model. The pressure on the lower surface of the airfoil was greater than that of the incoming
flow stream and as a result it effectively “pushed” the airfoil upward, normal to the incoming flow stream. On the other hand, the components of the pressure distribution parallel to the incoming flow stream tended to slow the velocity of the incoming flow relative to the airfoil, as do the viscous stresses.

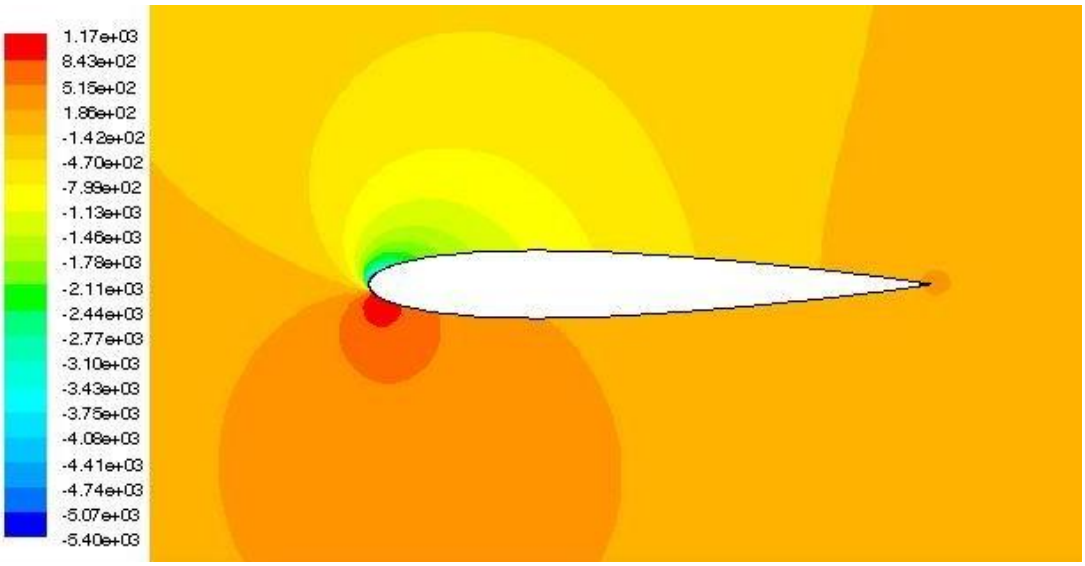

Figure 9. Contours of static pressure at 9° angle of attack with the Spalart – Allmaras turbulence model.

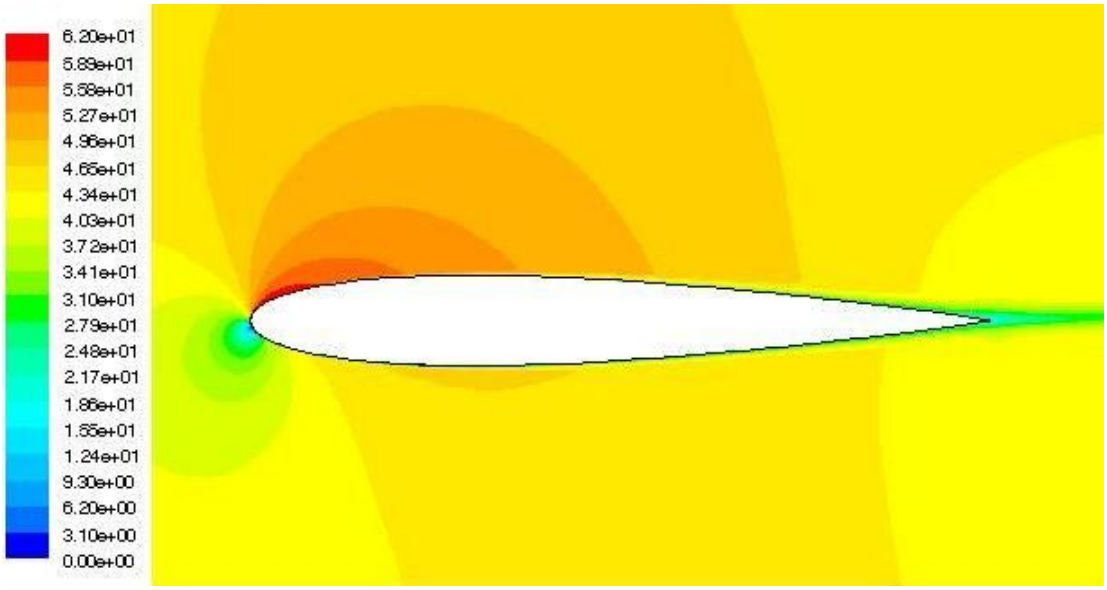

Figure 10. Contours of velocity magnitude at 3° angle of attack with the Spalart-Allmaras turbulence model.

Contours of velocity components at angles of attack 3, 9 and 16° are also shown (Figures 10, 11 and 12). The trailing edge stagnation point moved slightly forward on the airfoil at low angles of attack and it jumped rapidly to leading edge at stall angle. A stagnation point is a poimt in a flow field where the local velocity of the fluid is zero.

The upper surface of the airfoil experienced a higher velocity compared to the lower surface. That was expected from the pressure distribution. As the angle of attack increased the upper surface velocity was much higher than the velocity of the lower surface. Figure 13 shows the stagnation point for various angles of attack.

Conclusions

This paper showed the behaviour of the 4-digit symmetric airfoil NACA 0012 at various angles of attack. The most appropriate turbulence model for these simulations was the $k-\omega$ SST two-equation model, which had a good agreement with the published experimental data of other investigators for a wider range of angles of attack. The predicted drag coefficients were higher than the existing experimental data from reliable sources. This overprediction of drag was expected since the actual airfoil has laminar flow over the forward half. The

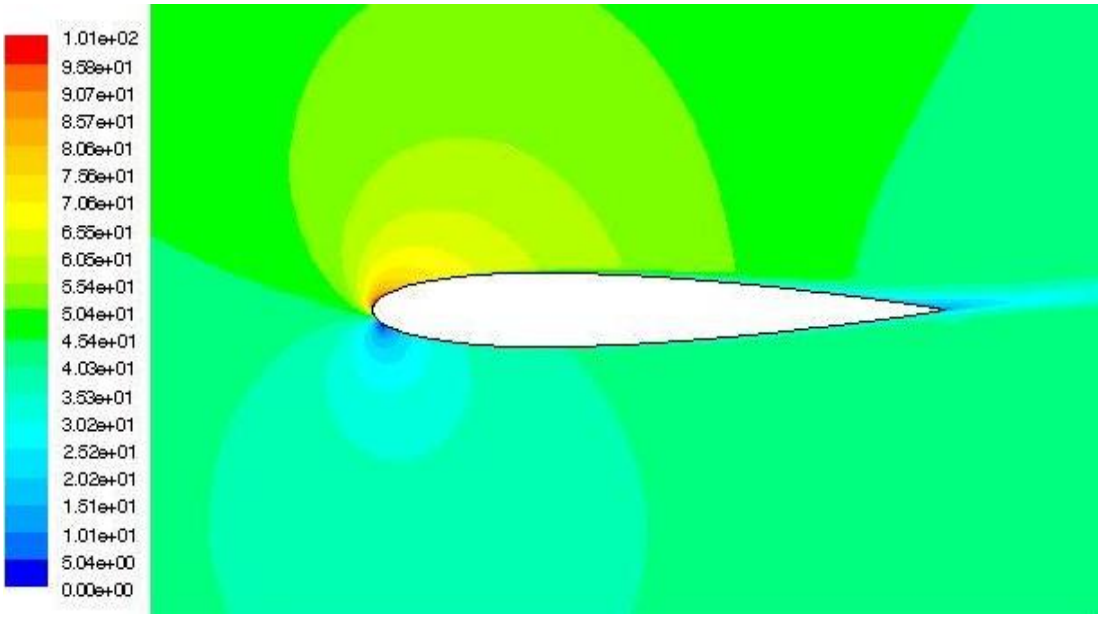

Figure 11. Contours of velocity magnitude at 9° angle of attack with the Spalart-Allmaras turbulence model.

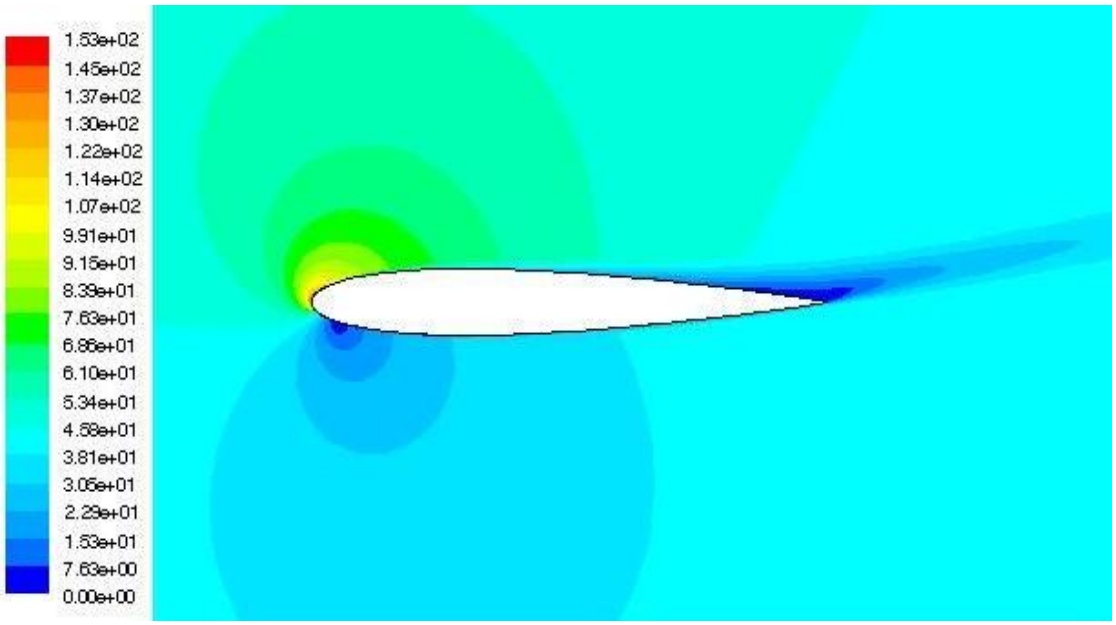

Figure 12. Contours of velocity magnitude at 16° angle of attack with the Spalart-Allmaras turbulence model.

computational results from the three turbulence models were compared with experimental data where the boundary layer formed around the airfoil is fully turbulent and they agreed well. Afterwards, the transition point from laminar to turbulent regime was predicted, the computational grid split in two regions, a laminar and a turbulent region, and then new simulations were realized. By this method, the computational results agreed very well with corresponding experimental data.

ACKNOWLEDGEMENTS

This research was co-financed by the European Union (European Social Fund – ESF) and Greek national funds through the Operational Program "Education and Lifelong Learning" of the National Strategic Reference Framework (NSRF) - Research Funding Program: Heracleitus II. Investing in knowledge society through the European Social Fund.

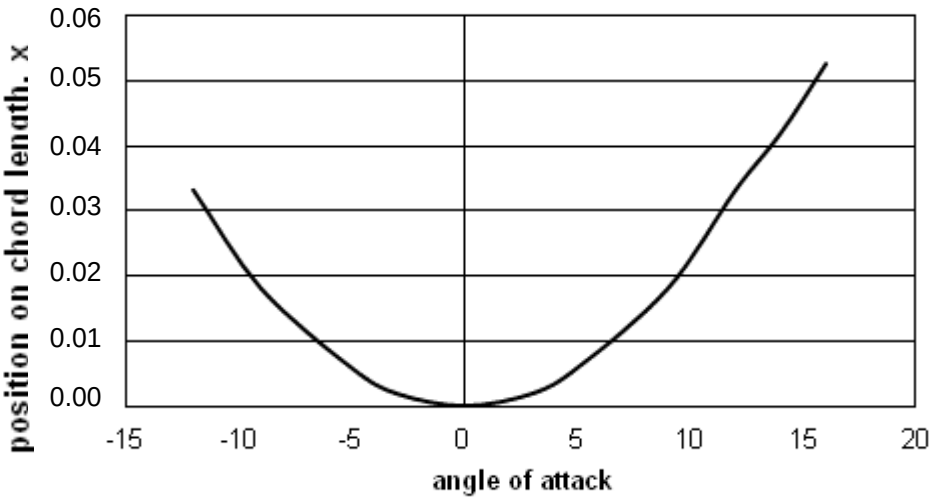

Figure 13. Stagnation point for various angles of attack.

REFERENCES

Abbott IH, Von Doenhoff AE (1959). Theory of Wing Sections. Dover Publishing, New York.

Bacha WA, Ghaly WS (2006). Drag Prediction in Transitional Flow over Two-Dimensional Airfoils, Proceedings of the 44th AIAA Aerospace Sciences Meeting and Exhibit, Reno, NV.

Badran O (2008). Formulation of Two-Equation Turbulence Models for Turbulent Flow over a NACA 4412 Airfoil at Angle of Attack 15 Degree, 6th International Colloquium on Bluff Bodies Aerodynamics and Applications, Milano, 20-24 July.

ANSYS (2006). ANSYS Fluent 6.3.26.

Johansen J (1997). Prediction of Laminar/Turbulent Transition in Airfoil Flows. Risø National Laboratory, Roskilde, Denmark.

Launder BE, Spalding DB (1974). The numerical computation of turbulent flows. Comp. Meth. Appl. Mechanics Engr., 3: 269-89.

Ma L, Chen J, Du G, Cao R (2010). Numerical simulation of aerodynamic performance for wind turbine airfoils. Taiyangneng Xuebao/Acta Energiae Solaris Sinica, 31: 203-209.

McCroskey WJ (1987). A Critical Assessment of Wind Tunnel Results for the NACA 0012 Airfoil. U.S. Army Aviation Research and Technology Activity, Nasa Technical Memorandum, 42: 285-330.

Menter FR (1994). Two-Equation Eddy-Viscosity Turbulence Models for Engineering Applications. AIAA J., 32: 1598-1605.

Shih TH, Liou WW, Shabbir A , Zhu J (1995). A new k-ε eddy – viscosity model for high Reynolds number turbulent flows – model development and validation. Computers Fluids, 24: 227-238.

Silisteanu PD, Botez RM (2010). Transition flow occurrence estimation new method. 48th AIAA Aerospace Science Meeting. Orlando, Floride, Etats-Unis, Janvier, pp. 7-10

Spalart, PR, Allmaras SR (1992). A One-Equation Turbulence Model for Aerodynamic Flows. AIAA Paper, pp. 92-439.

Sutherland W (1893). The viscosity of gases and molecular force. Philosophical Magazine, S., 5, 36: 507-531.

Wilcox DC (1988). Re-assessment of the scale-determining equation for advanced turbulence models. AIAA J., 26: 1414-1421.